Northumbria Research Link

Singlemode-Multimode-Singlemode Optical Fiber Sensor for Accurate Blood Pressure Monitoring

Yi-Neng Pang, Bin Liu, Juan Liu, Sheng-Peng Wan, Tao Wu, Jinhui Yuan, Xiangjun Xin, Xing-Dao He and Qiang Wu

Abstract— A dual-channel single-mode-multi-mode-single-mode (SMS) fiber optic sensor encapsulated by polydimethylsiloxane (PDMS) was proposed for the first time, for the simultaneous monitoring of the brachial and radial arteries for accurate blood pressure prediction. With the help of the machine learning algorithm Support Vector Regression (SVR), the SMS fiber sensor can continuously and accurately monitor the systolic and diastolic blood pressure. Commercial sphygmomanometers are used to calibrate the accuracy of blood pressure measurement. Compared with the single-channel system, this system can extract more pulse wave features for blood pressure prediction, such as radial artery transit time (RPTT), brachial artery transit time (BPTT), and the transit time difference between the radial artery and the brachial artery (DBRPTT). The results show that the performance of dual-channel blood pressure monitoring is more accurate than that of single-channel blood pressure monitoring in terms of the absolute value of the correlation coefficient (R) and the average value of the difference between SBP and DBP. In addition, both the single-channel and dual-channel blood pressure monitoring are in line with the Association for the Advancement of Medical Devices (AAMI), but the average deviation (DM, 0.06 mmHg) and standard deviation (SD, 1.54 mmHg) of dual-channel blood pressure monitoring are more accurate. The blood pressure monitoring system has the characteristics of low cost, high sensitivity, non-invasive and capability for remote real time monitoring, which can provide effective solution for intelligent health monitoring in the era of artificial intelligence in the future.

Index Terms— Blood pressure monitoring, SMS fiber sensors, Optical fiber sensors, Healthcare monitoring, Human pulse wave

I. INTRODUCTION

HEART and blood diseases are becoming more and more threats to human health, especially hypertension is the most common [1]. Blood pressure (BP) reflects the degree of cardiovascular health and is a reliable indicator of the human cardiovascular system [2]. Due to the unhealthy diet and lack of exercise for many people, and due to the aging society, hypertension has become the main threat to the health of the elderly [3], and the problem of hypertension has become very common among the population. Problems such as increasing labor costs, increasing medical expenses, and shortages of medical staff have gradually surfaced [4]. Therefore, intelligent blood pressure monitoring is very important in daily life.

Commercial sphygmomanometers usually use inflatable cuff technology, the basic principle of which is mainly the oscillometric method, and the discomfort and inconvenience of measurement are major problems [5,6]. Therefore, in order to make blood pressure monitoring more comfortable, convenient and accurate, a large number of blood pressure monitoring solutions have been proposed. These techniques are mainly divided into photoplethysmogram (PPG) sensors, optical imaging and ultrasound technique. In 2019, Riaz et al. effectively realized the physiological relationship between the pulse width and the BP of the PPG signal through wearable PPG [7]. In 2019, Mousavi et al. proposed a new method that uses only the PPG signal without considering its shape to estimate mean arterial pressure (MAP), diastolic blood pressure (DBP), and systolic blood pressure (SBP) [8]. Luo et al. described a new technology based on smart phones, called transdermal optical imaging based on non-contact methods [9]. Wang et al. developed an ultrasound and stretchable device that fits the skin, captures blood pressure waveforms in deeply buried arteries and veins, and can continuously monitor cardiovascular events [10]. However, in the case of sweating on the skin surface, the accuracy of the PPG and skin-contact sensor will be decreased [11]. In addition, these sensors do not allow blood pressure monitoring in magnetic environment (for example, magnetic resonance imaging) [12].

With the development of optical fiber technology, optical fiber sensors are gradually being used in the field of smart healthcare [13]. For example, Bennett et al. introduced a new non-invasive vital signs sensing technology based on

multimode fiber optic sensors, which can be integrated into fabrics. The technology is based on tracking the point intensity changes of speckle patterns caused by optical mode interference due to fiber deformation [14]. Koyama et al. developed an optical fiber Bragg grating vital sensor by installing an FBG sensor at the pulsation point of a living body [15]. Haseda et al. introduced an FBG sensor made of plastic optical fiber (POF-FBG) to realize blood pressure monitoring [16]. In 2015 C. Leitão *et al.* proposed an FBG based portable pen-like optical fiber sensor for central arteries pulse waveform acquisition, which has disadvantage of high cost and complex demodulation method due to it wavelength extracting nature [17]. The authors further presented a non-invasive arterial pulse waveform monitoring by using POF sensor [18], which is low cost and simple demodulation, but relatively low sensitivity.

This paper presents a high accuracy blood pressure monitoring method using a singlemode-multimode-singlemode (SMS) fiber structure with the employment of dual-channel measurement scheme. SMS sensors were imbedded into BP belt to monitor the brachial and radial arteries of the human body. BP prediction is carried out by constructing a BP model by extracting pulse features. One male and one female volunteer participated in the 20-day pulse collection experiment. A comparison between the dual-channel BP monitoring based on Support Vector Regression (SVR) method and single-channel BP monitoring was conducted, where dual-channel BP monitoring has proved to have better measurement accuracy. This accurate and wearable non-invasive BP monitoring technology holds great promise for the prevention and diagnosis of hypertension and cardiovascular disease.

II. METHODS AND EXPERIMENTS

A. Human pulse wave introduction

The human pulse wave signal contains the physiological information of human health, especially the physiological information of the human cardiovascular system [19]. Therefore, the pulse wave signal of the human body can be used as the basis of medical diagnosis. Physical diseases such as hypertension can be identified by features such as pulse wave cycle, propagation speed, and the location of peaks and troughs. Therefore, pulse transit time, which refers to the time for arterial pressure wave to reach the surrounding vessels from the aortic valve during the ejection process of the heart artery, is a feature highly correlated with BP. Meanwhile, the pulse transit time, mainly affected by the size of the blood vessel and the elasticity of the blood vessel wall, is a common indicator reflecting the arterial elasticity and dilatability of the arteries. When BP rises, the blood vessel walls become tense and blood flow increases. When BP drops, vessel walls relax and blood flow slows [20]. In the experiment, two pulse waves (the radial artery and brachial artery of the arm) are selected as the sensing signals as shown in Figure 1. They are percussion waves (PW) and dicrotic waves (DW) in the basic pulse waves of the human body. By calculating the time points of the percussion wave and dicrotic wave, the following relevant parameters of blood pressure measurement can be obtained: the radial artery transit time (RPTT), the brachial artery transit time (BPTT) and the transit

time difference between the radial artery and the brachial artery (DBRPTT).
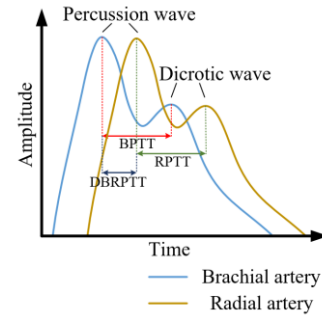
Figure 1. Typical brachial artery and radial artery pulse waveform with pulse transit time feature.

B. Sensing principle

The SMS fiber structure is configured by fusion splicing a short section of multimode fiber (MMF) between two singlemode fibers (SMFs), as shown in Figure 2. The SMS fiber structure utilizes multimode interferences within MMF, which has very high sensitivity for various applications, such as temperature, strain, refractive index, bio-chemical sensing [21-22]. Most recently we have studied the SMS fiber sensor for curvature and respiration state sensing [23]. The human circulatory system is composed of the heart, blood vessels and blood, and is responsible for transporting oxygen, carbon dioxide, nutrients and waste. The blood is squeezed into the aorta by the contraction of the left ventricle of the heart, and then flows to the arteries throughout the body. Arteries are tubes of elastic connective tissue and muscle. When a large amount of blood enters the arteries, the pressure increases and the diameter of the artery expands, and the pulse signal is felt by the arteries on the surface of the body [24]. The SMS fiber sensor is attached to the skin surface of human arteries (the human radial artery and brachial artery were selected for this BP sensing experiment because they are located on the human arm, which is convenient for measurement). The vibration signal caused by pulse wave causes deformation of SMS fiber sensor. Since the SMS fiber sensor is very sensitive to the bend [25-27], the output power of the SMS fiber sensor changes with the same pace as that of the pulse wave, and thus can be used to measure BP.
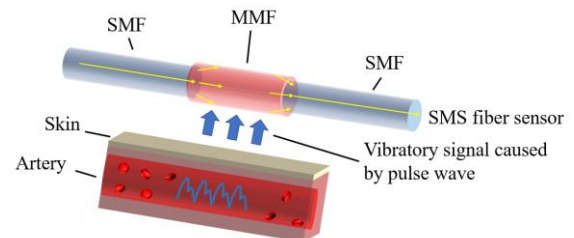
Figure 2. SMS optical fiber sensor structure and pulse sensing principle

C. Experimental setup

The SMS fiber sensor was made by connecting 30 mm MMF to SMF using fusion splicer (Fujikura 80C). Since the SMS optical fiber sensor is fragile, the SMS fiber sensor is encapsulated with PDMS as shown in Figure 3(b). The thickness of the PDMS coating and elastic belt are 3 mm and 2 mm, respectively. The thickness of PDMS coating is slightly larger than that of the elastic belt, which makes the SMS sensor closely attached to

the human skin (brachial and radial artery), and thus has better sensitivity. The PDMS encapsulated SMS fiber sensor is then embedded into two elastic fabrics as shown in Figure 3 (a), where a rectangular hole (40 mm×5 mm) is cut in the middle of each elastic fabric. The SMS fiber sensor is placed in the holes of two elastic fabrics and then stitch the two elastic fabrics together. This configuration enables the PDMS encapsulated SMS fiber sensor has direct contact with the skin surface and thus improve sensitivity. Figure 3(c) shows the picture of the packaged SMS BP elastic belt. Figure 4 shows a schematic diagram of the BP monitoring system, which is composed of a CW (Continuous Wave) laser (1550 nm), two SMS BP elastic belts (one is placed in radial artery, another one is placed in brachial artery), two InGaAs photodiodes (PDA10CS-EC, THORLABS), an optical fiber splitter (WLF-102-001), a FPGA (Field Programmable Gate Array) voltage acquisition unit and a PC (Personal Computer). It is noted that the miniaturization and low cost is the driving force for technology development [28]. To realize this goal, the light source and PDs proposed in this paper can be replaced by low-cost light source and photodiode, such as LSFLD155 laser diode and LSIPD-A75 photodiode made from Beijing Light-sensing Technologies LTD, where the whole system could be as low as $30.
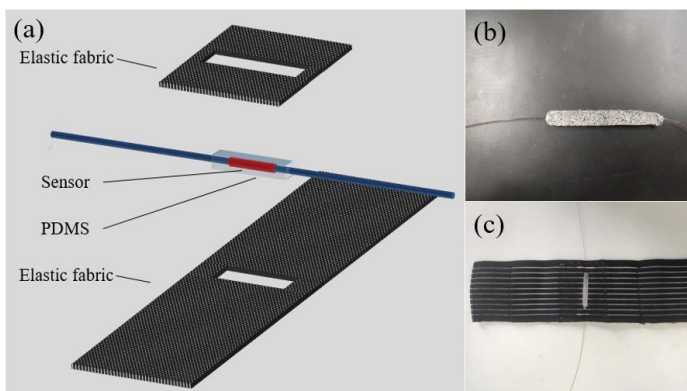
Figure 3. (a) Schematic diagram of an optical fiber BP elastic belt; image of (b) SMS fiber sensor encapsulated with PDMS; (c) BP elastic belt embedded with SMS fiber sensor**.**
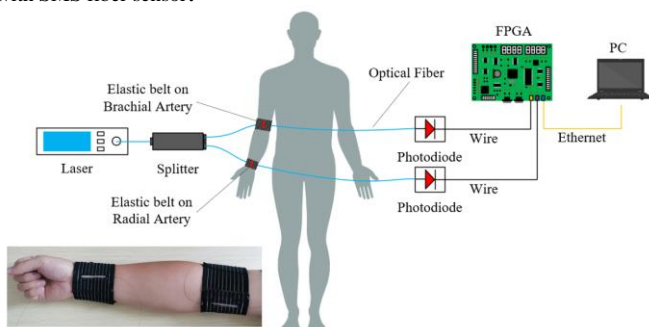

Figure 4. Schematic diagram of the BP monitoring experimental setup.

D. Collection and preprocessing of measured pulse

Pulse transit time is the core parameter to predict the BP changes of individuals [29]. In our experiments, two healthy volunteers (one male, 26 years old; one female, 25 years old) were selected to participate in the measurement. Both volunteers signed the informed consent form, which has been approved by the university ethics committee. In the experimental data collection, a commercial BP meter (OMRON,

HEM-7211) is used as the true value of the experimental data. The experimental measurement data was collected continuously for 20 days, and pulse samples were taken 5 times a day (sampling time points: 9:00, 12:00, 15:00, 18:00, 21:00), and each measurement time was 10 seconds. The specific acquisition procedure is: 1) place the optical fiber elastic belt on the radial artery and brachial artery of the right hand; 2) use the FPGA signal acquisition system to acquire two-channel pulse signals at a 1 kHz acquisition rate; 3) place a commercial sphygmomanometer on the left upper arm. The measurement was performed in a sitting position, with both hands on the table, keeping the same level with the heart to improve measurement accuracy. In order to achieve the purpose of BP prediction, the raw pulse signal denoising and feature extraction is processed on the original pulse signal as shown in Figure 5. The yellow solid line is Brachial Artery Wave (BAW), and the blue solid line is Radial Artery Wave (RAW). First, in the signal preprocessing step in the Figure 5(a-b), wavelet decomposition is used to remove the baseline interference and noise of the original signal (the wavelet generating function used in the paper is db4 and the wavelet decomposition is level 5) [30], The pulse wave period is segmented according to the location of the trough in the Figure 5(c), the red dotted line is Brachial artery Cycle Segmentation (BCS), and the green dotted line is Radial artery Cycle Segmentation (RCS). Then the peak value search method is used to search for the location of the percussion and dicrotic wave in the Figure 5(d) [31]. The red prototype presents Brachial artery Percussion Wave (BPW), the green prototype presents Brachial artery Dicrotic Wave (BDW), The red triangle presents Radial artery Percussion Wave (RPW), and the green prototype presents Radial artery Dicrotic Wave (RDW). Finally, effective judgments were made for signals that could not find the percussion wave peak and the dicrotic wave peak in the Figure 5(e). Signals with an effective signal ratio greater than or equal to 50% were retained, while those with an effective signal ratio less than 50% were removed. In the experiment, among 100 groups of male volunteers' signals, 82 groups of valid signals were retained and 18 groups of invalid signals were removed; among 100 groups of female volunteers' signals, 72 groups of valid signals were retained and 28 groups of invalid signals were removed. According to the principle that 80% of the signals are used as BP modeling signals and 20% of the signals as BP test signals. From the valid signals of male volunteers, 66 sets of signals were selected as BP modeling signals, and the remaining 16 sets of signals were used as BP test signals. From the valid signals of female volunteers, 58 sets of signals were selected as BP modeling signals, and the remaining 14 sets of signals were used as BP test signals.
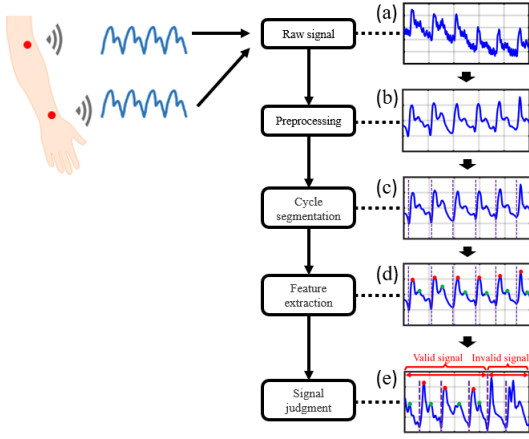
Figure 5. Human pulse signal processing and feature extraction workflow

E. The blood pressure estimation model

• *BP monitoring based on single-channel SMS fiber sensing*

In a single-channel measurement, the relationship between pulse transit time and blood pressure is shown in Eq. (1) [32]:

$$BP = K_a \, ln(PTT) + K_b \frac{1}{PTT^2} + K_c \qquad (1)$$

where BP is either the Systolic Blood Pressure (SBP) or the Diastolic Blood Pressure (DBP), PTT is either the RPTT or the BPTT, Ka, Kb, and Kc are the parameters of the single-channel BP model as shown in the Table I. As shown in the Table I, the performance of the single-channel BP model is revealed by the Goodness of Fit (R2). The results the R^2 of the brachial artery is smaller than that of the radial artery, which is due to the fact that the pulse intensity of the brachial artery is smaller than that of the radial artery, resulting in an increase in measurement error.

Table I Parameter and performance of single-channel blood pressure model

Subject	Location	BP	K_a	K_b	K_c	R^2
male	Radial artery	SBP	-235.3	-4794000.0	1507.0	0.74
		DBP	-178.3	-3289000.0	1104.0	0.67
	Brachial artery	SBP	-92.0	-964100.0	651.8	0.51
		DBP	-79.9	-732700.0	518.3	0.51
female	Radial artery	SBP	-14.8	165100.0	166.9	0.63
		DBP	-25.8	-246400.0	205.3	0.55
	Brachial artery	SBP	-38.3	-415700.0	307.6	0.57
		DBP	-44.0	-701800.0	314.6	0.53

• *BP monitoring based on dual-channel SMS fiber sensing*

In dual-channel SMS fiber sensing, Support Vector Machines (SVM) algorithm is used for BP monitoring. The SVM is suitable for both classification and regression applications. The regression or the function approximation version of SVM is called support vector machine-regression (SVR) [33], which is considered as a maximum-margin algorithm. Since predicting BP is a regression problem, common machine learning regression algorithms include linear regression, deep learning, and SVR [34]. Although the linear regression algorithm is relatively simple, it is not good at dealing with nonlinear problems. Deep learning can handle nonlinear problems but requires large number of data. SVR is good at handling nonlinear problems with small samples with excellent generalization effect and application range [35], compared to other machine learning algorithms. Since the amount of pulse data collected in this paper is 100 sets per person, which is neither very large nor linear, SVR was selected to predict BP. We have a set of training samples $\{(x_i, y_i), i = 1,2,\cdots,n\}$, the expected output $y_i \in R, x_i \in R^n$, $f(x) \le \omega, x \ge b$ is used for fitting (x_i, y_i) using the linear ε insensitive loss function [36-37]:

$$|f(x) - y|_\varepsilon = \begin{cases} 0 & |f(x) - y| \le \varepsilon \\ |f(x) - y| - \varepsilon & \text{others} \end{cases} \qquad (2)$$

Add relaxation factor $\xi_i \ge 0$ and $\xi_i^* \ge 0$, Then the above problem becomes a constraint condition:

$$\begin{cases} y_i - f(x_i) \le \varepsilon + \xi_i \\ f(x_i) - y_i \le \varepsilon + \xi_i^* \end{cases} \quad i = 1, 2, \cdots, n \qquad (3)$$

Minimizing objective function:

$$\varphi(w, \xi_i, \xi_i^*) = \frac{1}{2}|w|^2 + c\sum_{i=1}^n(\xi_i + \xi_i^*) \qquad (4)$$

where c is the punish coefficient, the dual problem of the above problems can be obtained by using the optimization algorithm: the constraint,

$$\begin{cases} \sum_{i=1}^n(\alpha_i - \alpha_i^*) = 0 \\ \alpha_i \ge 0, \alpha_i^* \le c \end{cases} \quad i = 1, 2, \cdots, n \qquad (5)$$

maximize the objective function for the Lagrange factor α_I, α_I^*

$$W(\alpha, \alpha^*) = -\varepsilon\sum_{i=1}^n(\alpha_i + \alpha_i^*) + \sum_{i=1}^n(\alpha_i - \alpha_i^*) - \frac{1}{2}\sum_{i,j=1}^n(\alpha_i - \alpha_i^*)(\alpha_j - \alpha_j^*)\langle x_i, x_j\rangle \qquad (6)$$

The value of α is solved to get the regression model:

$$f(x) = \langle w, x\rangle + b = \sum_{i=1}^n(\alpha_i - \alpha_i^*)\langle x_i, x\rangle + b \qquad (7)$$

For the nonlinear regression problem, data is mapped to a high-dimensional feature space by nonlinear mapping, which is transformed into a linear problem of high-dimensional space:

$$f(x) = \sum_{i=1}^n(\alpha_i - \alpha_i^*)K(x_i, x_j) + b \qquad (8)$$

The kernel function is Radial Basis Function (RBF):

$$K(x_i, x_j) = exp(-g\|x_i - x_j\|^2) \qquad (9)$$

Where g is kernel radius. Therefore, in this model, the settings of c and g are critical, and grid search is used to find the optimal c and g. Figure 7 shows an example of grid search for c and g, the x-coordinates, the y-coordinate and z- coordinate are log2c, log2g and Mean Square Error (MSE) respectively. The best c among the male volunteers SBP, the male volunteers DBP, the female volunteers SBP and the female volunteers DBP were 996.9987, 173.6454, 377.4129 and 263.1971, respectively. The best g among the male volunteers SBP, the male volunteers DBP, the female volunteers SBP and the female volunteers DBP were 0.0037, 0.0501, 0.0012 and 0.0010, respectively.
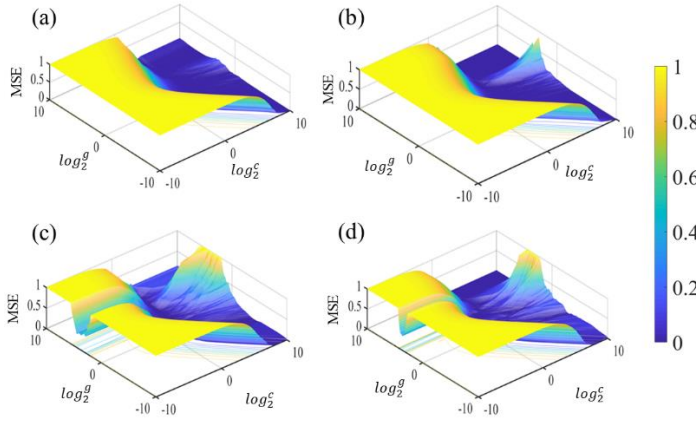
Figure 6. Grid search for c (punish coefficient) and g (kernel radius) in (a) the male volunteer SBP model, (b) the male volunteer DBP model, (c) the female volunteer SBP model and (d) the female volunteer SBP model.

III. RESULTS AND DISCUSSION

The test data including 16 groups collected from the male volunteer and the 14 groups collected from the female volunteer were analyzed by correlation plots and Bland-Altman plots. Figure 7 gives an example of the signal measured by the developed fiber sensor and processed using the above model. Figure 7(a) and (b) are raw signals detected by the SMS fiber sensor and pre-processed signals after removing the baseline and noise, respectively. Figure 7(c) shows BCS and RCS identified by cycle segmentation based on the position of the trough of the processed signal. Four points (BPW, RPW, BDW and RDW) of each cycle of the BAW and RAW were identified by the peak seeking algorithm in the Figure 7(d). A valid signal is defined as having a shock wave peak and a dicrotic wave peak in one pulse period, in which the shock wave is earlier than the dicrotic wave and the amplitude of the shock wave is higher than that of the dicrotic wave. In Figure 7(e), there is one pulse period is identified as invalid signal because only a dicrotic wave was identified in BAW and RAW respectively, all other pulse periods are valid signals. Correlation plots indicate the correlation analysis of the measured BP against the reference values [38]. The Bland-Altman plot was chosen to provide a more accurate comparison of the measurement by the dual-channel and single-channel BP monitoring [39], which was used to evaluate the consistency of the measurement results. Figures 8-10 show the Correlation plots and Bland-Altman plots of both the male and female volunteers' SBP and DBP based on radial artery, brachial artery and SVM respectively. The horizontal coordinate of the Bland-Altman plot is the mean of the measured BP and the reference BP (MMR), and the vertical coordinate is the difference between the measured BP and the reference BP (DMR). The solid black line in the graph represents the mean value of the DMR (MDMR), the closer it is to zero the better the agreement. The purple dashed line represents the 95% confidence interval, Mean ± 1.96 SD where the Mean is the MDMR and SD is the standard deviation, which becomes the 95% limits of agreement (LoA).
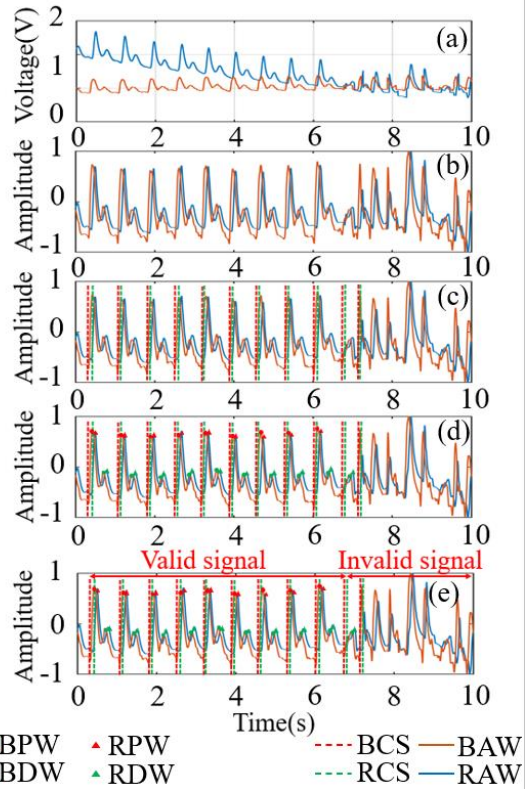
Figure 7. An example of measured pulse signal and its processing progress (a) Raw signal, (b) Preprocessing, (c) Cycle segmentation, (d) Feature extraction and (e) Signal judgment
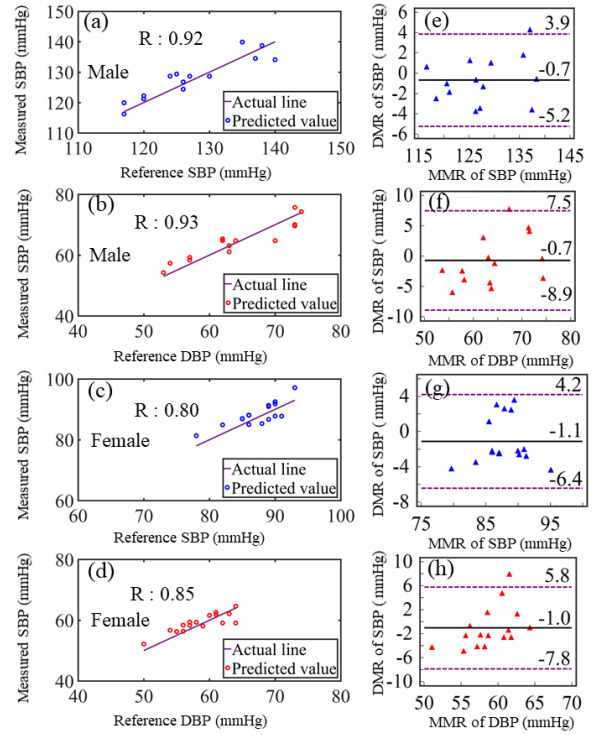
Figure 8. Single-channel blood pressure monitoring based on radial artery detecting: correlation plots and Bland-Altman plots of (a) (e) the male volunteer SBP, (b) (f) the male volunteer DBP, (c) (g) the female volunteer SBP and (d) (h) the female volunteer DBP.
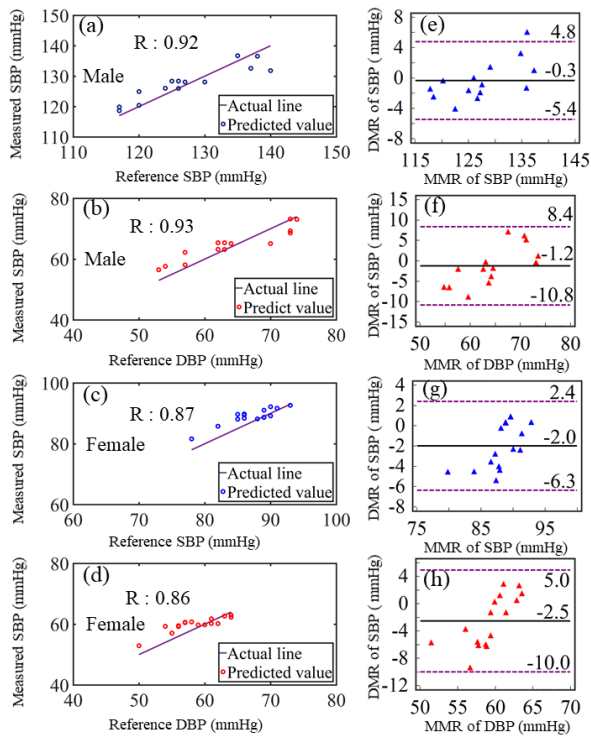
Figure 9. Single channel blood pressure monitoring based on brachial artery detecting: correlation plots and Bland-Altman plots of (a) (e) the male volunteer SBP, (b) (f) the male volunteer DBP, (c) (g) the female volunteer SBP and (d) (h) the female volunteer DBP.
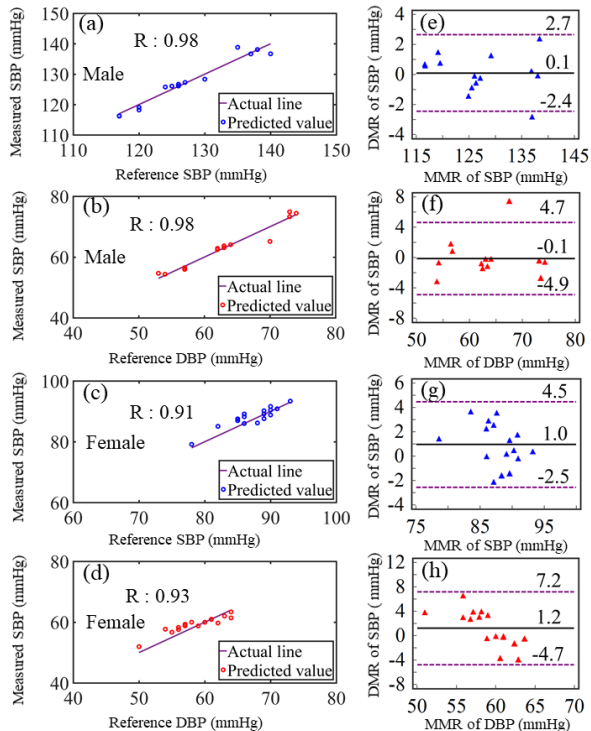
Figure 10. Dual-channel blood pressure based on SVM: correlation plots and Bland-Altman plots of (a) (e) the male volunteer SBP, (b) (f) the male volunteer DBP, (c) (g) the female volunteer SBP and (d) (h) the female volunteer DBP.

As displayed in the Figure 8 and Figure 9, Correlation Coefficient (R) and the MDMR of radial artery and brachial artery single-channel detecting are very close in SBP and DBP for both the male and female volunteers, the maximum

difference of the R and the MDMR between radial and brachial artery monitoring were 0.07 and 1.5 mmHg. However, the R of the female volunteer is smaller and the absolute of the MDMR of the female volunteer is greater than that of the male volunteer, the maximum difference of the R and the MDMR between the male volunteer and the female volunteer were 0.12 and 1.7 mmHg, which is possibly because the pulse intensity of female volunteer is weaker than that of the male and thus higher measurement error. From the Figure 10, the R of dual-channel detecting is greater than that of single-channel detecting in both SBP and DBP whose value for male volunteer are 0.98 and 0.91 respectively, and for female the SBP and DBP are 0.98 and 0.93 respectively. The absolute of the MDMR of dual-channel detecting is smaller than that of single-channel detecting. For both single-channel and dual-channel monitoring, the calculated points are basically within the purple line, which means that there is good consistency in measurements. The error of dual-channel BP monitoring model is lower than that of single-channel BP monitoring model in terms of the correlation plot and the Bland-Altman plots.

Table II summarized the calculated SBP and DBP in the Figures 8-10. As listed in Table II, The Association for the Advancement of Medical Instrumentation (AAMI) has two indicators for BP measurement device: Dm and SD [40]. In the results of this experiment, the Dm and SD of all three methods met the requirement of the AAMI, but the absolute value of Dm and SD in method 3 was smaller than that of the method 1 and 2, indicating that the method 3 has the best performance. The summarized results in Table II showed that both the single-channel and dual-channel BP monitoring met the standard of AAMI, but the result of the dual-channel BP monitoring was more accurate than that of the single-channel BP monitoring, with a minimum Deviation mean (Dm)/minimum Standard Deviation (SD) of 0.06/1.54 mmHg for dual-channel BP monitoring and 0.31/2.07 mmHg for single-channel BP monitoring.

Table II Comparison of experimental results between single-channel and dual-channel optical fiber sensing. Method 1: single -channel BP monitoring based on radial artery detecting; Method 2: single -channel BP monitoring based on brachial artery detecting; Method 3: dual-channel BP based on SVR; Dm: Deviation mean; SD: Standard deviation

Subject	Method	SBP		DBP		Dm±SD in AAMI (mmHg)
		Dm (mmHg)	SD (mmHg)	Dm (mmHg)	SD (mmHg)	
A(male)	1	0.81	3.05	0.33	2.65	5±8
	2	0.31	3.30	0.57	3.07	
	3	**-0.12**	**1.66**	**0.06**	**1.54**	
B(female)	1	0.97	2.50	0.54	2.07	
	2	1.70	2.52	1.41	2.56	
	3	**0.83**	**1.71**	**0.66**	**1.84**	

In order to verify the long-term stability and repeatability of the system, the BP of the two volunteers were measured after 10 months, and the experimental results calculated by method 3 show that the maximum Dm and SD are 1.66, 3.19 respectively. Compared with the data in Table II (0.83 and 1.84 respectively), we can conclude that both are within the standard

of AAMI, demonstrating good long-term stability and repeatability of the develop BP monitoring system.

Table III summarized the performance of the proposed BP sensor with other latest reported BP monitoring systems. Compared with other systems, the BP monitoring in this paper has advantages such as high measurement accuracy and Immunity to electromagnetic interference. It is noted that, like other types of BP systems, the SMS fiber BP system is only suitable for static measurement.

TABLE III
COMPARISON TABLE

Sensor Type	Sensor Location	SBP Accuracy (Dm, SD)	DBP Accuracy (Dm, SD)	Immunity to EI	Ref.
PPG	Radial artery	-0.05, 8.90	0.19, 4.17	No	[8] (2019)
OI	face	0.39, 7.30	-0.20, 6.00	No	[9] (2019)
PPG	Finger tips	0.06, 7.08	0.01, 4.66	No	[41] (2016)
OFCD	Radial artery	0.24, 2.39	0.12, 2.62	Yes	[32] (2020)
SMS sensor	Radial artery and Brachial artery	-0.12, 1.66	0.06, 1.54	Yes	This work

PPG = Photoplethysmograph, OI = Optical Imaging, OFCD = Optical Fiber Composite Diaphragm, EI = Electromagnetic Interference.

IV. CONCLUSION

In this study, we developed an optical fiber vibration sensor based dual-channel BP monitoring system for accurate BP detection. The SMS optical fiber sensors were embedded inside fabric belts to monitor the brachial and radial arteries of the human body. SVR were established to predict SBP and DBP by achieving RPTT, BPTT and DBRPTT from measured radial and brachial pulse waves, and a commercial BP meter was used to calibrate the BP. Based on the calculation of BP using a single feature (RPTT or BPTT) formula single-channel BP monitoring is compared with dual-channel BP monitoring, which collects radial artery and brachial artery signals respectively. The experiment results showed that dual-channel BP monitoring was more accurate than single-channel BP monitoring. Both single-channel and dual-channel BP monitoring were studied and compared in correlation plots and Bland-Altman plots. From the R and the MDMR, the measured PB by dual-channel is more accurate than that by single-channel. The R of dual-channel BP monitoring is up to 0.98 and the minimum of the absolute of the MDMR in dual-channel BP monitoring is 0.1. The experimental results showed that both single-channel and dual-channel BP monitoring were in line with AAMI standards, but the dual-channel BP monitoring was more accurate with the mean deviation (Dm) and standard deviation (SD) of 0.06 mmHg and 1.54 mmHg, respectively. This work provides a simple, accurate and user-friendly method to monitor BP, which has important implications for the monitoring of hypertension and supports the future development of smart healthcare.

REFERENCES

[1] B. Schumann, A. Seidler, A. Kluttig, K. Werdan, J. Haerting and K. H. Greiser, "Association of occupation with prevalent hypertension in an elderly East German population: an exploratory cross-sectional analysis," *International Archives of Occupational and Environmental Health,* vol. 84, no. 4, pp. 361-369. Apr. 2011.

[2] S. Chaising, P. Temdee, P, "Determining Significant Risk Factors for Preventing Elderly People with Hypertension from Cardiovascular Disease Complication Using Maximum Objective Distance," Wireless Personal Communications, vol. 115, pp. 3099-3122, Dec. 2020

[3] B. Guo, Z. Shi, W. Zhang, H. Zhao, K. He, X. Hu, Y. Gan, S. Shi and Q. Tian, "Trajectories of body mass index (BMI) and hypertension risk among middle-aged and elderly Chinese people," *J Hum Hypertens*, vol. 35, pp. 537-545, Jun. 2021.

[4] Y. Song, J. Li, B. István, R. Xuan and Y. Gu, "Current evidence on traditional Chinese exercises for quality of life in patients with essential hypertension: a systematic review and meta-analysis," *Frontiers in Cardiovascular Medicine*, vol. 7, Jan. 2021.

[5] I. Baran Akkuş, F. Kavak Akelma, M. Emlek, D. Özkan, J. Ergil and R. Polat, "Comparison of the standard and triple airway maneuvering techniques for i-gel™ placement in patients undergoing elective surgery: a randomized controlled study," *J Anesth*, vol. 34, pp. 512-518, Aug. 2020.

[6] T. Anbarasan, A. Rogers, D. A. Rorie, J. W. K. Grieve, T. M. MacDonald and I. S. Mackenzie, "Home blood pressure monitors owned by participants in a large decentralised clinical trial in hypertension: the Treatment In Morning versus Evening (TIME) study," *J Hum Hypertens*, Feb. 2021.

[7] F. Riaz, M. A. Azad, J. Arshad, M. Imran, A. Hassan and S. Rehman, "Pervasive blood pressure monitoring using Photoplethysmogram (PPG) sensors," *Future Generation Computer Systems*, vol. 98, pp. 120-130, Sep. 2019.

[8] S. S. Mousavi, M. Firouzmand, M. Charmi, M. Hemmati, M. Moghadam and Y. Ghorbani, "Blood pressure estimation from appropriate and inappropriate PPG signals using a whole-based method," *Biomedical Signal Processing and Control*, vol. 47, pp. 196-206, Jan. 2019.

[9] H. Luo, D. Yang, A. Barszczyk, N. Vempala, J. Wei, S. J. Wu, P. P. Zheng, G. Fu, K. Lee and Z. Feng, "Smartphone-based blood pressure measurement using transdermal optical imaging technology," Circulation-Cardiovascular Imaging, vol. 12, no. 8, Aug. 2019.

[10] C. Wang, X. Li, H. Hu, L. Zhang, Z. Huang, M. Lin, Z. Zhang, Z. Yin, B. Huang, H. Gong, S. Bhaskara, Y. Gu, M. Makihata, Y. Guo, Y. Lei, Y. Chen, C. Wang, Y. Li, T. Zhang, Z. Chen, A. P. Pisano, L. Zhang, Q. Zhou and S. Xu, "Monitoring of the central blood pressure waveform via a conformal ultrasonic device," Nature biomedical engineering, vol. 2, no. 9, pp. 687-695, Sep. 2018.

[11] L. Kalevo, T. Miettinen, A. Leino, S. Kainulainen, K. Myllymaa, J. Töyräs, T. Leppänen and S. Myllymaa, "Improved sweat artifact tolerance of screen-printed EEG electrodes by material selection-comparison of electrochemical properties in artificial sweat," *IEEE Access*, vol. 7, pp. 133237-133247, Sep. 2019.

[12] P. Roriz, L. Carvalho, O. Frazão, J. L. Santos, and J. A. Simões, "From conventional sensors to fibre optic sensors for strain and force measurements in biomechanics applications: A review," J. Biomech., vol. 47, no. 6, pp. 1251–1261, 2014.

[13] C. Massaroni, M. Zaltieri, D. Lo Presti, A. Nicolo, D. Tosi, and è. Schena, "Fiber Bragg Grating Sensors for Cardiorespiratory Monitoring: A Review," *IEEE Sensors Journal*, pp: 1-1, 2020.

[14] A. Bennett, Y. Beiderman, S. Agdarov, Y. Beiderman, R. Hendel, B. Straussman and Z. Zalevsky, "Monitoring of vital bio-signs by analysis of speckle patterns in a fabric-integrated multimode optical fiber sensor," Optics Express, vol. 28, no. 14, pp. 20830-20844, Feb. 2020.

[15] S. Koyama, T. Hayase, S. Miyauchi, A. Shirai, S. Chino, Y. Haseda and H. Ishizawa, "Influence on measurement signal by pressure and viscosity changes of fluid and installation condition of FBG Sensor using blood

flow simulation model," *IEEE Sensors Journal,* vol. 19, no. 24, pp. 11946-11954, Dec. 2019.

[16] Y. Haseda, J. Bonefacino, H. Tam, S. Chino, S. Koyama and H. Ishizawa, "Measurement of pulse wave signals and blood pressure by p plastic optical fiber FBG sensor," Sensors, vol. 19, p. 5088, Nov. 2019.

[17] C. Leitão, P. Antunes, P. André, J. L. Pinto and J. M. Bastos, "Central arteries pulse waveform acquisition with a portable pen-like optical fiber sensor," Devices and Technology, vol. 20, pp. 43-46, 2015.

[18] C. Leitáo, P. Antunes, J. M. Bastos, J. L. Pinto and P. André, "Plastic optical fiber sensor for noninvasive arterial pulse waveform monitoring," IEEE Sensors Journal, vol. 15, no. 1, pp. 14-18, Jan. 2015.

[19] L. Stoner, D. Lambrick, J. Faulkner and J. M. Young, "Guidelines for the use of pulse wave analysis in adults and children," Journal of atherosclerosis and thrombosis, vol. 20, no. 4, pp. 404-406, Jan. 2013.

[20] I. Z. Apostolakis, G. M. Karageorgos, P. Nauleau, S. D. Nandlall and E. E. Konofagou, "Adaptive Pulse Wave Imaging: automated spatial vessel wall inhomogeneity detection in phantoms and in-vivo," IEEE transactions on medical imaging, vol. 39, no. 1, pp. 259-269, Jan. 2020.

[21] Q. Wu, Y. Semenova, P. F. Wang and G. Farrell, "High sensitivity SMS fibre structure based refractometer-analysis and experiment," Optics Express, vol. no. 19, pp. 7937-7944, 2011.

[22] Q. Wu, Y. W. Qu, J. Liu, J. H. Yuan, S. P. Wang, T. Wu, X. D. He, B. Liu, D. J. Liu, Y. Q. Ma, Y. Semenova, X. J. Xin, P. Wang and G. Farrell, "Singlemode-Multimode-Singlemode fibre Structures for Sensing Applications - A Review," IEEE Sensors Journal, vol. 21, no. 11, pp. 12734-12751, 2021.

[23] Y. N. Pang, B. Liu, J. Liu, S. P. Wan, T. Wu, X. D. He, J. Yuan, X. Zhou, K. Long, and Q. Wu, "Wearable optical fiber sensor based on a bend singlemode-multimode-singlemode fiber structure for respiration monitoring", IEEE Sensors Journal, Oct. 2020.

[24] C. Martin J, R. Donald L and M. Tofy, "Development of a mathematical model of the human circulatory system," Annals of Biomedical Engineering, vol. 34, no. 9, pp. 1400-1413, Aug. 2006.

[25] X. Li, D. Liu, R. Kumar, W. P. Ng, Y. Q. Fu, J. Yuan, C. Yu, Y. Wu, G. Zhou, G. Farrell, Y. Semenova, and Q. Wu, "A simple optical fiber interferometer based breathing sensor", *Measurement Science and Technology*, vol. 28, no. 3, 2017

[26] Q. Wu, M. Yang, J. Yuan, H. P. Chan, Y. Ma, Y. Semenova, P. Wang, C. Yu, and G. Farrell, "The use of a bend singlemode-multimode-singlemode (SMS) fiber structure for vibration sensing", *Optics and Laser Technology*, vol. 63, pp. 29-33, 2014

[27] Q. Wu, Y. Semenova, P. Wang, A. M. Hatta, and G. Farrell, "Experimental demonstration of a simple displacement sensor based on a bent single-mode–multimode–single-mode fiber structure", *Measurement Science and Technology*, 22 025203 (2011).

[28] A. G. Leal-Junior, C. R. C. R. Díaz, C. Leitão, M. J. M. J. Pontes, C. Marques, and A. Frizera, "Polymer optical fiber-based sensor for simultaneous measurement of breath and heart rate under dynamic movements," *Optics and Laser Technology*, vol. 109, pp. 429–436, Aug. 2018.

[29] JI. Davies and AD. Struthers, "Pulse wave analysis and pulse wave velocity: a critical review of their strengths and weaknesses," Journal of hypertension, vol. 21, no. 3, pp. 463-472, 2003.

[30] JL. Starck, J. Fadili and F. Murtagh, "The undecimated wavelet decomposition and its reconstruction," IEEE transactions on image processing, vol. 16, no. 2, pp. 297-309, Feb. 2007.

[31] C. Si, W. Wang, Z. Hui and J. Wang, "A fast peak-searching algorithm for ultrasonic elastography," Journal of Ultrasound in Medicine, vol. 36, no. 8, pp. 1707-1721, Aug. 2017.

[32] L. Li, Y. Li, L. Yang, F. Fang, Z. Yan and Q. Sun, "Continuous and accurate blood pressure monitoring based on wearable optical fiber wristband," IEEE Sensors Journal, vol. 21, pp. 1-1, Sep. 2020.

[33] A.J. Smola, B. Scholkopf, "A tutorial on support vector regression," Statistics and Computing, vol. 14, no. 3, pp. 199-222, 2004.

[34] I. Goodfellow, Y. Bengio, A. Courville, Deep Learning. Massachusetts, USA. MIT Press, 2016, pp. 98-155.

[35] CJC. Burges, A Tutorial on Support Vector Machines for Pattern Recognition. Data Mining & Knowledge Discovery, vol. 2, no. 2, pp. 121-167, 1998.

[36] V. Cherkassky and Y Ma, "Practical selection of SVM parameters and noise estimation for SVM regression," Neural Networks, vol. 17, no. 1, pp. 113-126, Jan. 2004.

[37] W. Rasheed and T. B. Tang, "Anomaly detection of moderate traumatic brain injury using auto-regularized multi-instance one-class SVM," IEEE Transactions on Neural Systems and Rehabilitation Engineering, vol. 28, no. 1, pp. 83-93, Jan. 2020.

[38] R. H. Wang, J. Zhao, Y. Sun, H. Yu, N. Zhou, H. X. Zhang, and D. G. Jia, "Wearable respiration monitoring using an in-line few-mode fiber Mach-Zehnder interferometric sensor," *Biomedical Optics Express*, vol. 11, no. 1, pp. 316-329, Jan. 2020.

[39] PS. Myles and J. Cui, "Using the Bland-Altman method to measure agreement with repeated measures," British Journal of Anaesthesia, vol. 3, pp. 309-311, 2007.

[40] E. O'Brien, F. Mee, N. Atkins and K. O'Malley, "Evaluation of the SpaceLabs 90202 non-invasive ambulatory recorder according to the AAMI Standard and BHS criteria," Journal of Human Hypertension, vol. 5, no. 3, pp. 223-226, 1991.

[41] X. Xing and M. Sun, "Optical blood pressure estimation with photoplethysmography and FFT-based neural networks," Biomedical Optics Express, vol. 7, no. 8, p. 261929, Aug. 2016.

Yi-Neng Pang received the B.S. degree from Hunan Institute of Engineering in 2017. He is currently pursuing the M.S. degree in optical engineering with Nanchang Hangkong University. His current research interests include optical fiber sensing and signal processing.

Bin Liu received his B.S. and Ph.D. degree from Sun Yat-sen University, China. Dr. Liu is an associate Professor with Key Laboratory of Nondestructive Test (Ministry of Education) of Nanchang Hangkong University, China. His main research interest is fiber optic sensing.

Juan Liu received her Ph.D. degree from Beijing Normal University, China. She is an associate Professor with Key Laboratory of Nondestructive Test (Ministry of Education) of Nanchang Hangkong University, China. Her main research interest is fiber optic sensing.

Sheng-Peng Wan received the B.S. and Ph.D. degrees from University of Electronic and Technology of China. He is a professor with Key Laboratory of Nondestructive Test (Ministry of Education) of Nanchang Hangkong University, China. His main research interest is fiber optic sensing.

Tao Wu received his Ph.D. degree in Optics from University of the Littoral Opal Coast and Anhui Institute of Optics and Fine Mechanics, China. In 2010, Dr. Wu joined Key Laboratory of Nondestructive Test (Ministry of Education) of Nanchang Hangkong University, China. His main research interest has been the development of high-sensitivity laser spectrometer for laboratory and field studies of atmospheric trace gases and aerosols.

Jinhui Yuan received the Ph.D. degree in physical electronics from Beijing University of Posts and Telecommunications (BUPT), Beijing, China, in 2011. He is currently a Professor at the Department of computer and communication engineering, University of Science and Technology Beijing (USTB). He was selected as a Hong Kong Scholar at the Photonics Research Centre, Department of Electronic and Information Engineering, The Hong Kong Polytechnic University, in 2013. His current research interests include photonic crystal fibers, silicon waveguide, and optical fiber devices. He is the Senior Members of the IEEE and OSA. He has published over 200 papers in the academic journals and conferences.

Xing-Dao He was born in Jingan, Jiangxi Province, China, in 1963. He received the Ph.D. degree in optics from Beijing Normal University, Beijing, China, in 2005. He is currently a Professor with the Key Laboratory of Nondestructive Test (Ministry of Education), Nanchang Hangkong University, China. His current research interests include light scattering spectroscopy, optical holography, and information processing.

Qiang Wu received the B.S. and Ph.D. degrees from Beijing Normal University and Beijing University of Posts and Telecommunications, Beijing, China, in 1996 and 2004, respectively. From 2004 to 2006, he worked as a Senior Research Associate in City University of Hong Kong. From 2006 to 2008, he took up a research associate post in Heriot-Watt University, Edinburgh, U.K. From 2008 to 2014, he worked as a Stokes Lecturer at Photonics Research Centre, Dublin Institute of Technology, Ireland. He is an Associate Professor/Reader with Faculty of Engineering and Environment, Northumbria University, Newcastle Upon Tyne, United Kingdom. His research interests include optical fiber interferometers for novel fiber optical couplers and sensors, nanofiber, microsphere sensors for bio-chemical sensing, the design and fabrication of fiber Bragg grating devices and their applications for sensing, nonlinear fibre optics, surface plasmon resonant and surface acoustic wave sensors. He has over 200 publications in the area of photonics and holds 3 invention patents. He is an Editorial Board Member of Scientific Reports, an Associate Editor for IEEE Sensors Journal and an Academic Editor for Journal of Sensors.